Article

Synthesis of N-Doped ZnO Nanocomposites for Sunlight Photocatalytic Degradation of Textile Dye Pollutants

Rowshon Kabir, Md. Abu Khalid Saifullah, Abrar Zadeed Ahmed, Shah Md. Masum and Md. Ashraful Islam Molla *

Department of Applied Chemistry & Chemical Engineering, Faculty of Engineering & Technology, University of Dhaka, Dhaka 1000, Bangladesh; rkabir1123173@gmail.com (R.K.); badhonks56@gmail.com (M.A.K.S.); zadeed.sibaat@gmail.com (A.Z.A.); masumdhk@yahoo.com (S.M.M.)
* Correspondence: ashraful.acce@du.ac.bd

check for
updates

Abstract: Undoped and N-doped ZnO nanocomposites are produced by a simple and low-cost mechanochemical method. The characterizations of all nanocomposites are examined by X-ray diffraction (XRD), Fourier transform-infrared (FT-IR), scanning electron microscopy (SEM) and UV-Vis-NIR spectroscopy. The XRD measurements show that the crystal sizes of undoped and N-doped ZnO nanocomposites are ~29 and ~28 nm, respectively. The UV-Vis-NIR spectroscopy results illustrate that the transmittance of the 7 wt% N/ZnO in the visible and infrared region is a bit higher than the undoped ZnO. The photocatalytic activity of undoped and N-doped ZnO nanocomposites is investigated for the degradation of Methylene Blue (MB) and Rhodamine B (RhB) aqueous solution with direct sunlight irradiation. The photocatalytic degradation percentages with 7 wt% N/ZnO for 5 and 10 mg/L MB dye solution are found to be 93.70% and 98.11%, respectively, whereas 78.40% and 89.15% degradation percentages are found with undoped ZnO, after 3 h sunlight irradiation. Under the same conditions, the photocatalytic degradation value of RhB dye (10 mg/L) solution is measured to be 86.21% for 7 wt% N/ZnO and 64.75% for undoped ZnO. The N-doped ZnO nanocomposites are found to exhibit enhanced photocatalytic performance for both dyes' degradation under sunlight irradiation in comparison with the undoped ZnO. Therefore, the photocatalytic degradation treatment of wastewater including dye pollutants with sunlight is an easy and simple technique, and cost-effective.

Keywords: N-doped ZnO; nanocomposite; photocatalytic degradation; sunlight; mechanochemical method

1. Introduction

Semiconductor photocatalysts have been employed to degrade organic dye pollutants because of their intrinsic properties [1]. Apart from various semiconductors, zinc oxide (ZnO) is one kind of the important semiconductor photocatalysts because of its unique advantages, such as low price, high photocatalytic activity, stability and nontoxicity [2]. ZnO is considered to be the first choice semiconductor photocatalyst due to its large quantum efficiency [3]. It can be applied for adsorption, solar cells, field emission devices, lithium-ion batteries, pressure transducers and photocatalysis [4–6]. Several studies have reported the effectiveness of ZnO for photocatalytic degradation of organic compounds such as textile dye [7]. Photocatalytic degradation of the toxic dyes using solar energy has attracted considerable interest for environmental protection [8]. However, owing to the large energy band gap (3.3 eV), ZnO can be only activated under UV light radiation [9]. Hence, to harvest more solar energy for photocatalysis, it is urgent to reduce the band gap of the ZnO. Doping with nonmetals can

be considered as a feasible approach to improve its utilization of solar energy and charge separation efficiency [10,11]. Among nonmetal dopants, nitrogen (N) is emerging as a key dopant element in different semiconductor oxides [12]. It is reported that the N atoms doping effectively improves the light absorption of ZnO in the visible range [13]. Klingshirn et al. have proved that N impurities act as shallow acceptors in ZnO thin films and bulk crystals [14].

Different methods have been developed to synthesize N-doped ZnO (N/ZnO) including the sol-gel process [15], hydrothermal process [16], wet chemical process [17], chemical vapor deposition [18], mechanochemical process [19] and high-energy milling [20]. The combustion reaction is a simple method for synthesizing N-doped ZnO which does not involve complicated, strictly controlled conditions and special equipment [21]. N/ZnO has been proven to be a good photocatalyst in the degradation of various organic dyes [22]. Prabakaran et al. have synthesized N/ZnO nanocomposites using a hydrothermal method and studied the photocatalytic degradation of methylene blue under UV and visible light [23]. Sudrajat et al. have prepared N/ZnO nanoparticles through a combustion reaction and investigated their application on the degradation of methylene blue [7]. Ma et al. have fabricated the N/ZnO photocatalysts via a simple heat-treatment and studied the photocatalytic activity [24].

The main purpose of this paper is to synthesize N-doped ZnO through a mechanochemical combustion reaction. Different weight percentages of urea have been used as a dopant source due to its low cost and easy handling. Furthermore, the photocatalytic ability of N-doped ZnO samples has been evaluated for the degradation of methylene blue (MB) and rhodamine B (RhB) under sunlight.

2. Materials and Methods

2.1. Chemicals

The samples were synthesized using zinc acetate dihydrate ($Zn(CH_3COO)_2 \cdot 2H_2O$), oxalic acid dihydrate ($(COOH)_2 \cdot 2H_2O$) and urea (H_4N_2CO). Methylene blue ($C_{16}H_{18}ClN_3S$) and Rhodamine B ($C_{28}H_{31}ClN_2O_3$) dye were employed in the photocatalytic degradation experiment. All of the chemicals were obtained from Merck (Darmstadt, Germany). All of the analytical grade chemicals were used without any purification. Deionized water was used for the preparation of solutions.

2.2. Synthesis Method

The controlled combustion method was used to synthesise the doped and N-undoped ZnO nanocomposites. Firstly 2.195 g of zinc oxalate dihydrate and 2.521 g of acetic acid were taken in an agitate mortar and ground for 10 min to produce $Zn(CH_3COO)_2 \cdot 2H_2O$ and $(COOH)_2 \cdot 2H_2O$ paste. The existence of acetic acid was observed by the presence of its typical smell. Then, for the doped ones, urea was added as a source of nitrogen and the grinding process continued for a further 10 min to obtain the precursor. The undoped and N-doped ZnO crystallites were obtained by calcination of the precursors at a temperature of 500 °C for 3 h under atmospheric conditions [25].

2.3. Characterization

The diffraction patterns of the as-synthesized samples were collected using a powder X-ray diffractometer (XRD, Ultima IV, Rigaku Corporation, Akishima, Japan) employing Cu Kα radiation (λ = 0.15406 nm, 40 KV, 1.64 mA) in 2θ angle range from 5° to 70°. The morphologies of undoped and N-doped ZnO were recorded with a scanning electron microscope (SEM, JSM-6010 PLUS/LA, JEOL Ltd., Tokyo, Japan). The chemical structures of the as-synthesized nanocomposites were studied using a Fourier transformed infrared (FTIR) spectrophotometer (IR Prestige-21, SHIMADZU, Tokyo, Japan) while the optical absorption spectra of the samples were measured by a UV–Vis-NIR spectrophotometer range from 300 nm to 1100 nm.

2.4. Evaluation of Photocatalytic Activity

The photocatalytic activities of undoped and N-doped ZnO nanocomposites were examined by the degradation of MB and RhB dye in aqueous solution under sunlight irradiation at ambient temperature. Typically, 30 mL of MB (5 and 10 mg/L) solution and 20 mg of synthesized photocatalyst were added to a 100 mL beaker as shown in Figure 1. Experiments were conducted under similar conditions on a sunny day between 11:00 and 14:00. To equilibrate the suspension, a magnetic stirrer was used in the dark for 30 min. Then, the suspensions in the beakers were kept in sunlight for different time intervals. About 3 mL MB solution was withdrawn and separated with an Advantec membrane filter 0.45 μm. The MB concentration was calculated using UV–visible spectrometry (UV-1700 Pharma Spec, SHIMADZU, Kyoto, Japan). The relative MB concentration (C/C_0) was determined at the relative absorbance (A/A_0) of $\lambda = 662$ nm, according to the Beer-Lambert law, where A_0 and A were the absorbance of aqueous MB at a starting time (t_0) of photocatalytic degradation and at any time t, respectively. The photocatalytic degradation of RhB (10 mg/L) solution was similar to that of MB except that the detection wavelength was 554 nm.
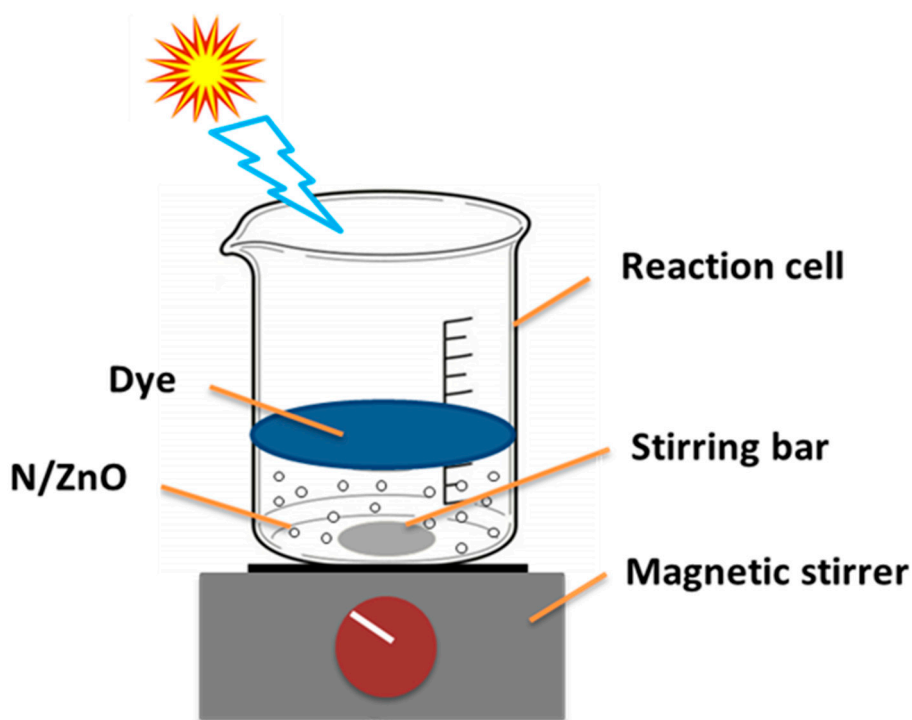

Figure 1. Schematic diagram of the reactor for photocatalytic degradation of dye.

3. Results and Discussion

3.1. XRD Patterns Study

Figure 2 displays the XRD patterns of undoped and N-doped ZnO nanocomposites. All the diffraction peaks can be indexed to the hexagonal wurtzite structure of ZnO (JCPDno.36-1451), proving that the resulting samples are pure ZnO [26]. It is obvious that the (100), (002) and (101) planes possess the highest intensities, indicative of an isotropic growth of the as-prepared ZnO. The diffraction peaks of the N-doped ZnO nanoparticles are also in good agreement with those of hexagonal ZnO (JCPDScard36-1451) and are almost identical to that of the pure ZnO, indicating that the N atoms have been doped in the ZnO crystal and no new phase has been formed [27]. The particle sizes of the undoped and N-doped ZnO nanocomposites have been obtained from the full width at half maximum (FWHM) of the most intense peaks of the respective crystals using the Scherrer equation, $D = 0.9\lambda/\beta\cos\theta$, where λ is the X-ray wavelength, D the average crystallite size, θ the Bragg diffraction angle and β the

full width at half-maximum. The crystal size of undoped and N-doped ZnO nanocomposites can be estimated as ~29 and ~28 nm, respectively.
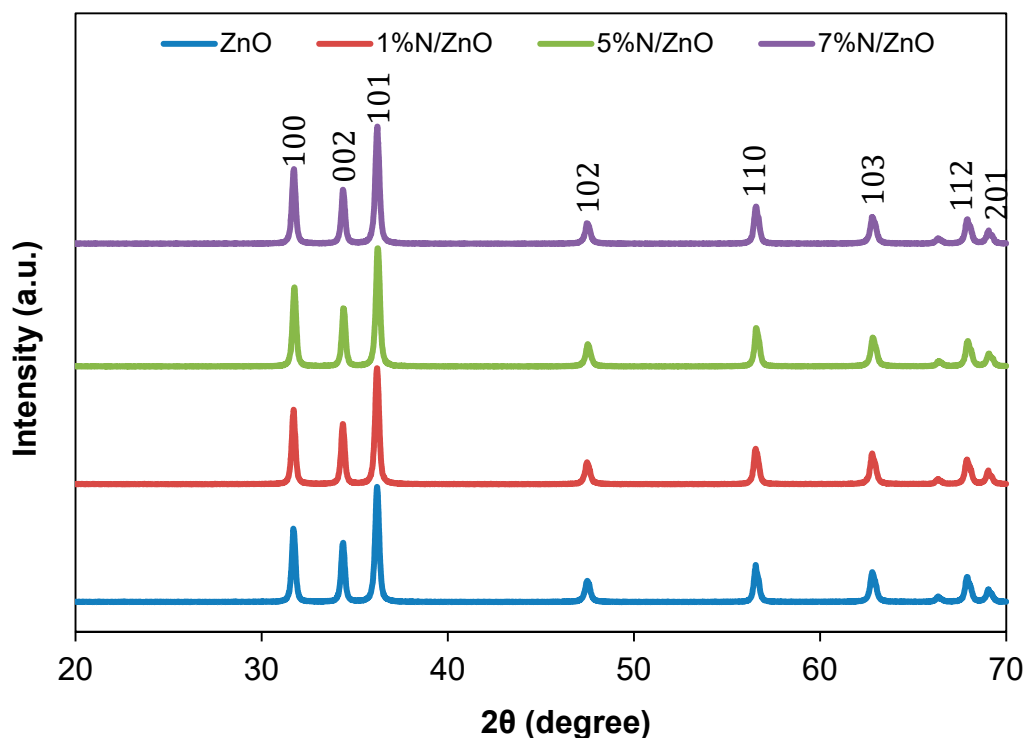
Figure 2. XRD patterns of undoped and N-doped ZnO nanocomposites.

3.2. SEM Study

Figure 3 presents the surface morphologies of the undoped and N-doped ZnO nanocomposites evaluated by SEM with different magnifications. The synthesized undoped ZnO is heterogeneous and distributed over the surface with the rod shape branches of building blocks shown in Figure 3a. As shown in the SEM image, N-doped ZnO nanocomposites are irregular structures and have a high degree of agglomeration. After doping N, the surface of N-doped ZnO particles becomes relatively smooth. The morphologies of N-doped ZnO nanocomposites are moderately different from the undoped ZnO. The average size of the particles observed by SEM is in the nanometer range, which is consistent with the XRD results. The particle size of N-doped ZnO seems to be smaller than that of undoped ZnO. This is also compatible with the XRD results.
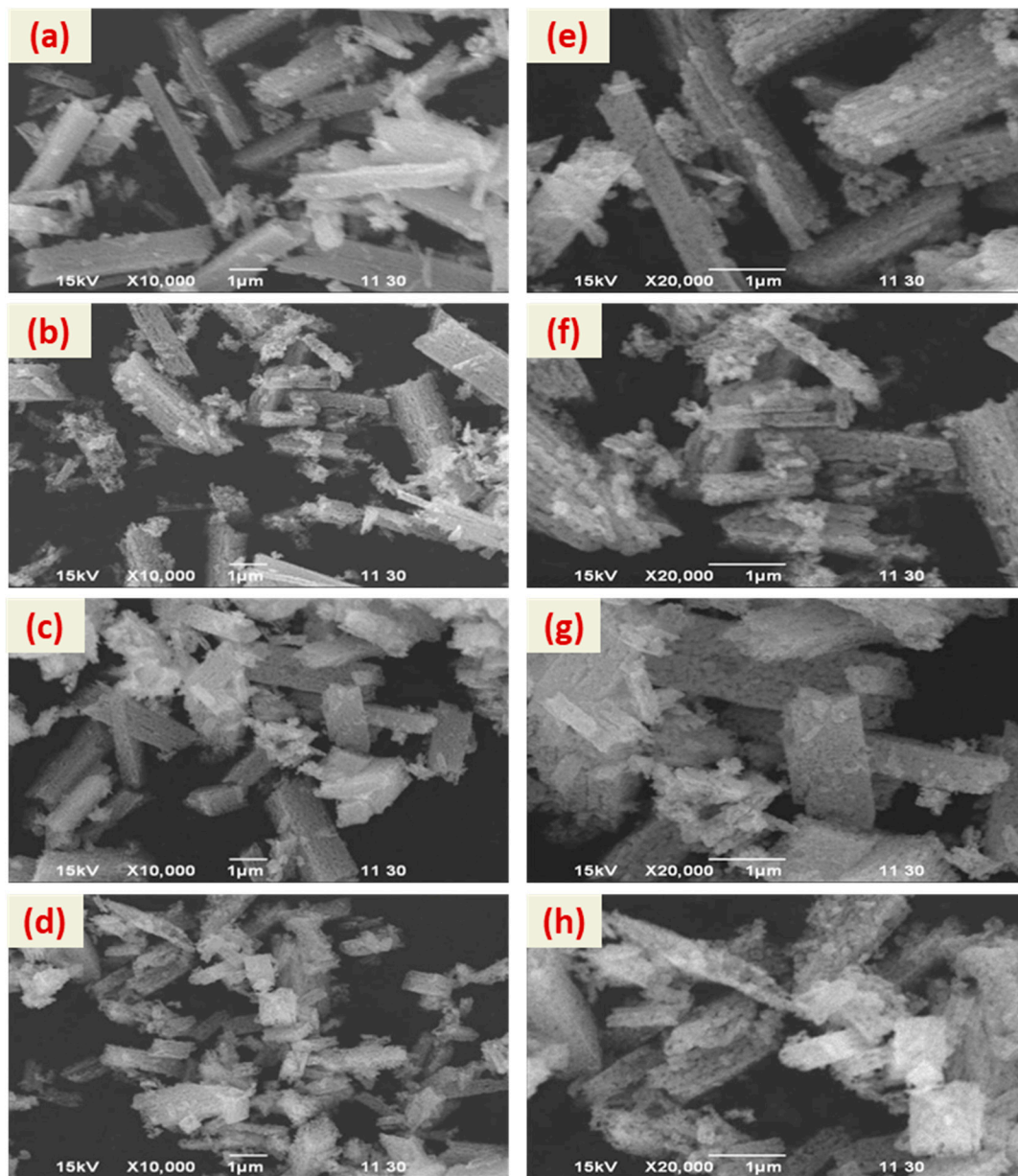
Figure 3. SEM images with different magnifications (**a**,**e**) ZnO, (**b**,**f**) 1% N/ZnO, (**c**,**g**) 5% N/ZnO and (**d**,**h**) 7% N/ZnO.

3.3. FT-IR Spectral Study

Figure 4 illustrates the FTIR results of undoped and N-doped ZnO nanocomposites. The IR spectra demonstrate that the zinc oxide absorption band with a stretching mode of Zn−O is between 400 cm^{-1} to 590 cm^{-1}, which corresponds to the hexagonal ZnO wurtzite crystal structure [28]. The stretching in the Zn–O bond is observed at around 480 cm^{-1} for N-doped ZnO whereas bond stretching appears at 441 cm^{-1} for undoped ZnO. After N doping, the Zn−O stretching peak splits into two components which are ascribed to the variation of the oxygen defect density [29]. The splitting degree of the Zn−O peak of N/ZnO is higher than that of ZnO; a higher density of oxygen defects in N/ZnO is expected. The oxygen defects, such as oxygen vacancies, are known to serve as electron traps which suppress electron-hole recombination [30], and thus are beneficial for improving the photocatalytic activity.
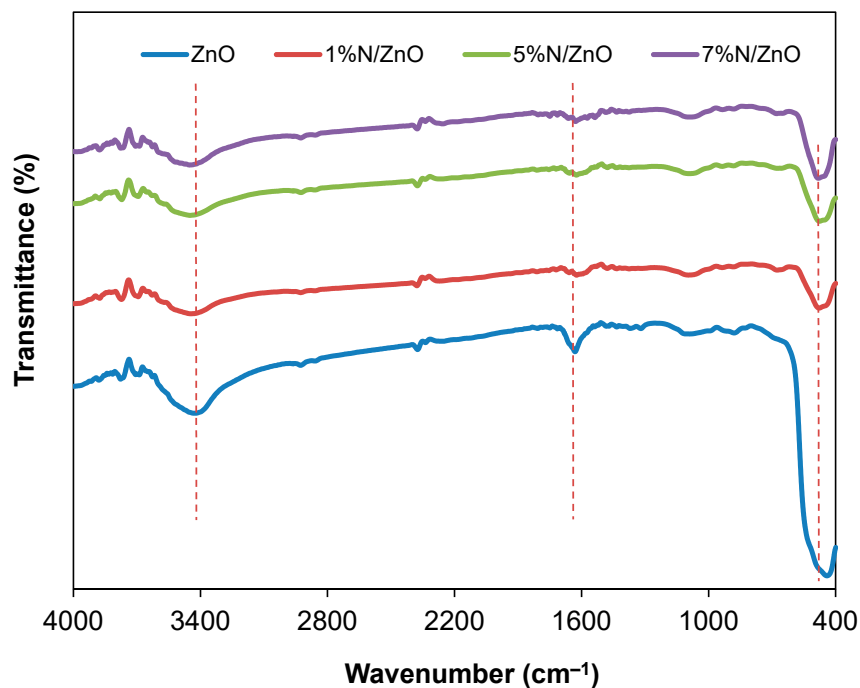
Figure 4. FTIR spectra of undoped and N-doped ZnO nanocomposites.

3.4. UV-Vis-NIR Study

Figure 5 illustrates the UV-Vis-NIR spectroscopy results of undoped and N-doped ZnO nanocomposites. As shown in Figure 5, the transmittance of the 7 wt% N/ZnO in the visible and infrared region is slightly higher than those of the ZnO. The higher transmittances of the ZnO than those of N/ZnO nanocomposites in the UV region are attributed to the higher band gap energy of ZnO than that of N/ZnO [31].
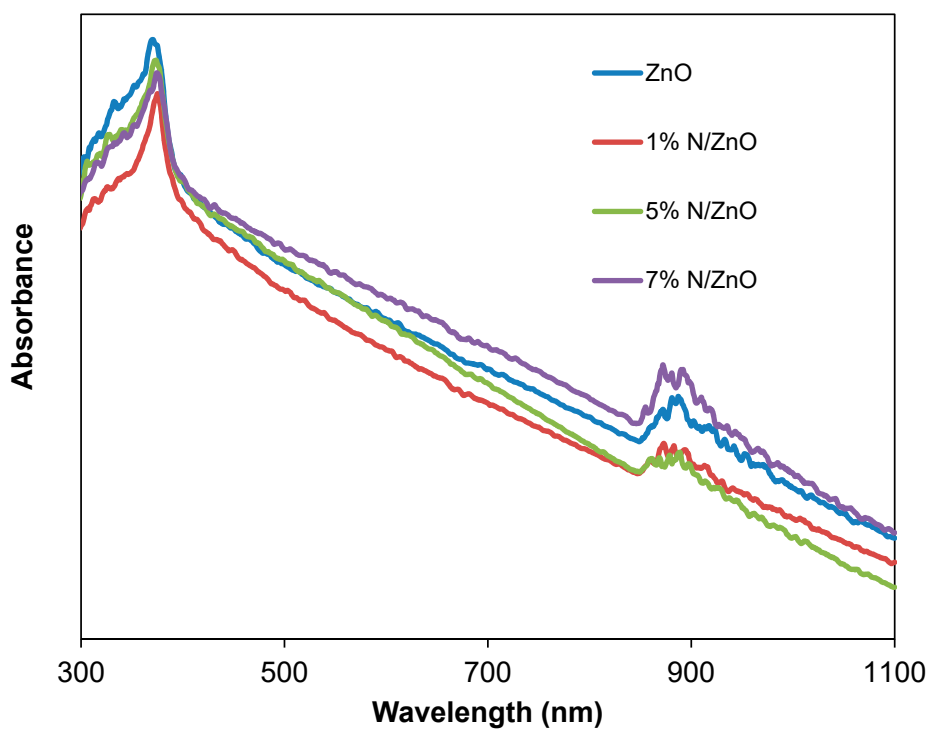

Figure 5. UV−Vis−NIR spectra of undoped and N-doped ZnO nanocomposites.
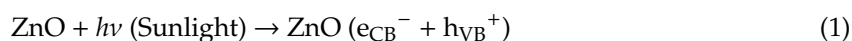
3.5. Photocatalytic Dye Degradation

Undoped and N-doped ZnO were used in the presence of sunlight for the degradation of MB and RhB to evaluate the photocatalytic performance. The effect of the dopants in the photocatalytic degradation of MB and RhB is depicted in Figure 6. The degradation percentage increases with increasing the amount of N doping, and 7 wt% doping in ZnO shows the highest degradation of dye. From Figure 6a, for 5 mg/L MB dye solution the photocatalytic degradation percentage with 7 wt% N/ZnO is 93.70% where the percentage without doping is 78.40% under sunlight irradiation within 3 h. Again for 10 mg/L MB dye solution, the photocatalytic degradation percentage with 7 wt% N/ZnO is 98.11% where the percentage without doping is 89.15% after 3 h sunlight irradiation. Under the same conditions, the degradation percentage of RhB dye of 10 mg/L solution is 86.21% with 7 wt % N/ZnO and 64.75% with undoped ZnO. The photodegradation percentage for MB and RhB dyes is congruous with the UV-Vis-NIR spectroscopy results. Furthermore, the N-doped ZnO nanocomposites are found to exhibit enhanced photocatalytic activity for both dyes' degradation under sunlight irradiation in comparison with the undoped ZnO. This is due to the improvement of the crystallinity of the N-doped ZnO nanocomposites, which can suppress the recombination of the photogenerated electrons and holes [27].
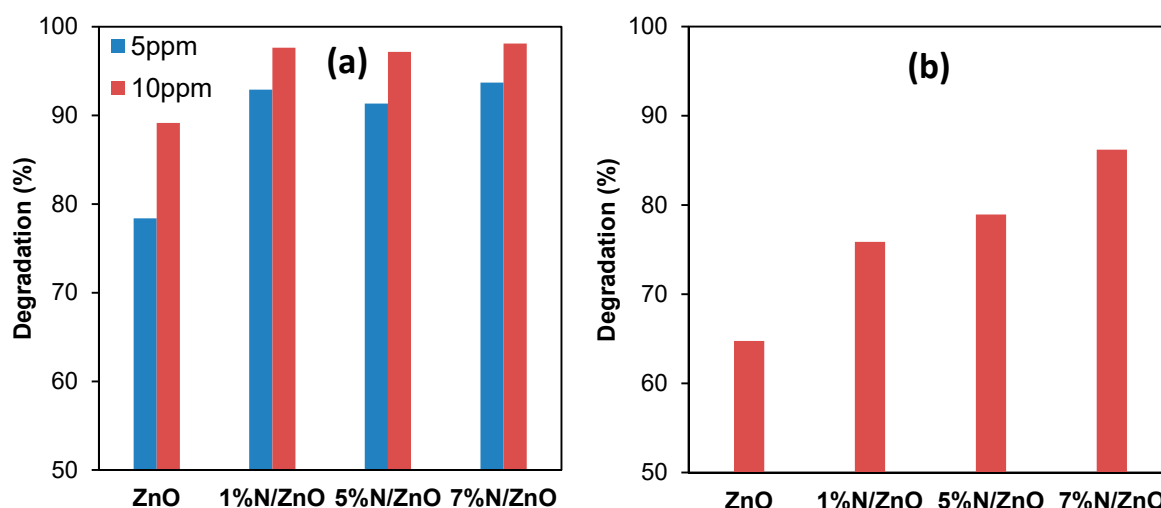

Figure 6. Percentages of photocatalytic degradation after 3 h' sunlight irradiation for (**a**) MB and (**b**) RhB dye.

3.6. Plausible Degradation Mechanism

The mechanism of the photocatalytic degradation of dye (RhB and MB) by N/ZnO with the sunlight irradiation is demonstrated in Figure 7. During the sunlight irradiation, the N/ZnO photocatalyst (3.1 eV) can easily absorb the light energy to create the conduction band electrons (e_{CB}^-) and valence band holes (h_{VB}^+) [8,23]. Then, the photoexcited e_{CB}^- interacts with dissolved oxygen (O_2) to generate a superoxide radical ($^\bullet O_2^-$) [32]. Besides, the photogenerated h_{VB}^+ can directly oxidize the organic dye (MB and RhB) to form degradation products or can react with the water (H_2O) to produce the hydroxide radical ($^\bullet OH$) [23,33]. Both radicals of $^\bullet O_2^-$ and $^\bullet OH$ are shown to be good oxidizing agents that readily attack the MB and RhB molecule to produce CO_2 and H_2O as end products. The plausible degradation reactions of dye (MB and RhB) with N/ZnO in the presence of sunlight in the photocatalytic system are described as follows [23,34].

$$ZnO + h\nu \text{ (Sunlight)} \rightarrow ZnO\ (e_{CB}^- + h_{VB}^+) \tag{1}$$

$$e_{CB}^- + O_2 \rightarrow {}^\bullet O_2^- \tag{2}$$

$$h_{VB}^+ + OH^- \rightarrow {}^\bullet OH \qquad (3)$$

$${}^\bullet O_2^- + Dye \rightarrow Degradation\ products \qquad (4)$$

$${}^\bullet OH + Dye \rightarrow Degradation\ products \qquad (5)$$

$$h_{VB}^+ + Dye \rightarrow Degradation\ products \qquad (6)$$
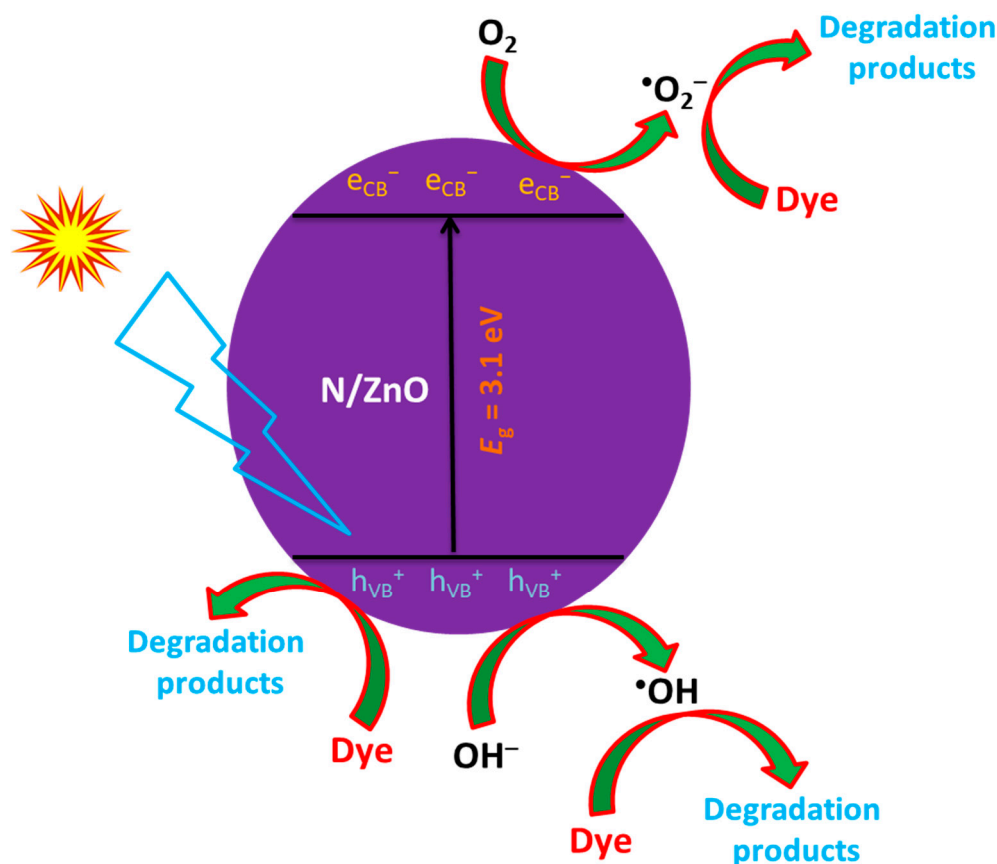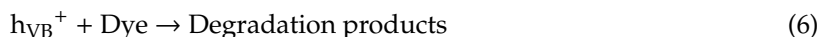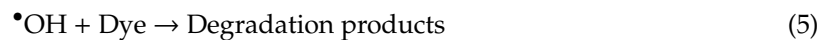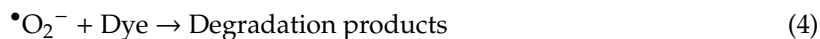
Figure 7. Schematic diagram of photocatalytic degradation mechanism of dye (RhB and MB) by N/ZnO with the sunlight irradiation.

4. Conclusions

N-doped ZnO nanocomposites have been synthesized using the mechanochemical method. The X-ray diffraction patterns of the samples show the formation of the ZnO phase as the main phase. The crystallite sizes of the samples confirm the nanometric sizes of the particles. The morphology reveals the formation of irregular shaped and soft agglomerates. From FTIR spectra, it is observed that the splitting degree of the Zn−O peak of N/ZnO is higher than undoped ZnO. In UV-Vis-NIR spectroscopy, the transmittance of the 7 wt% N/ZnO in the visible and infrared region is slightly higher than that of undoped ZnO. Hence, 7 wt% N/ZnO shows better photocatalytic dye degradation under sunlight irradiation. The photocatalytic degradation value of MB and RhB dye with N-doped ZnO is measured to be 98.11% and 86.21% respectively, after 3 h of sunlight irradiation. Therefore, the solar photocatalytic degradation technique may be a very effective method for the treatment of wastewater, including removing dye pollutants and improving the water quality of various natural sources.

Author Contributions: M.A.I.M. conceived and designed the experiments. R.K., M.A.K.S., A.Z.A. performed the experiments. R.K. wrote the original draft. M.A.I.M. edited the draft. S.M.M. analyzed the results. All authors have read and agreed to the published version of the manuscript.

References

1. Chen, M.; Guo, C.; Hou, S.; Lv, J.; Zhang, Y.; Zhang, H.; Xu, J. A novel Z-scheme AgBr/P-g-C$_3$N$_4$ heterojunction photocatalyst: Excellent photocatalytic performance and photocatalytic mechanism for ephedrine degradation. *Appl. Catal. B Environ.* **2020**. [CrossRef]
2. Zheng, Y.; Chen, C.; Zhan, Y.; Lin, X.; Zheng, Q.; Wei, K.; Zhu, J. Photocatalytic Activity of Ag/ZnO Heterostructure Nanocatalyst: Correlation between Structure and Property. *J. Phys. Chem. C* **2008**, *112*, 10773–10777. [CrossRef]
3. Zhua, D.; Zhou, Q. Action and mechanism of semiconductor photocatalysis on degradation of organic pollutants in water treatment: A review. *Environ. Nanotechnol. Monit. Manag.* **2019**, *12*, 100255. [CrossRef]
4. Meng, D.; Liu, D.; Wang, G.; Shen, Y.; San, X.; Si, J.; Meng, F. In-situ growth of ordered Pd-doped ZnO nanorod arrays on ceramic tube with enhanced trimethylamine sensing performance. *Appl. Surf. Sci.* **2019**, *463*, 348–356. [CrossRef]
5. Wang, R.; Chen, S.; Ng, Y.H.; Gao, Q.; Yang, S.; Zhang, S.; Peng, F.; Fang, Y.; Zhang, S. ZnO/CdS/PbS nanotube arrays with multi-heterojunctions for efficient visible-light driven photoelectrochemical hydrogen evolution. *Chem. Eng. J.* **2019**, *362*, 658–666. [CrossRef]
6. Guo, J.; Liao, X.; Lee, M.-H.; Hyett, G.; Huang, C.-C.; Hewak, D.W.; Mailis, S.; Zhou, W.; Jiang, Z. Experimental and DFT insights of the Zn-doping effects on the visible-light photocatalytic water splitting and dye decomposition over Zn-doped BiOBr photocatalysts. *Appl. Catal. B Environ.* **2019**, *243*, 502–512. [CrossRef]
7. Sudrajat, H.; Babel, S. A novel visible light active N-doped ZnO for photocatalytic degradation of dyes. *J. Water Process Eng.* **2017**, *16*, 309–318. [CrossRef]
8. Kong, J.-Z.; Zhai, H.-F.; Zhang, W.; Wang, S.-S.; Zhao, X.-R.; Li, M.; Li, H.; Li, A.-D.; Wu, D. Visible Light-Driven Photocatalytic Performance of N-Doped ZnO/g-C$_3$N$_4$ Nanocomposites. *Nanoscale Res. Lett.* **2017**, *12*, 526. [CrossRef]
9. Navale, Y.H.; Navale, S.T.; Stadler, F.J.; Ramgir, N.S.; Patil, V.B. Enhanced NO$_2$ sensing aptness of ZnO nanowire/CuO nanoparticle heterostructure-based gas sensors. *Ceram. Int.* **2019**, *45*, 1513–1522. [CrossRef]
10. Huo, P.W.; Zhou, M.J.; Tang, Y.F.; Liu, X.L.; Ma, C.C.; Yu, L.B.; Yan, Y.S. Incorporation of N-ZnO/CdS/Graphene oxide composite photocatalyst for enhanced photocatalytic activity under visible light. *J. Alloys Compd.* **2016**, *670*, 198–209. [CrossRef]
11. Kumar, S.G.; Rao Koteswara, K.S.R. Zinc oxide based photocatalysis: Tailoring surface-bulk structure and related interfacial charge carrier dynamics for better environmental applications. *RSC Adv.* **2015**, *5*, 3306–3351. [CrossRef]
12. Di Valentin, C.; Pacchioni, G. Spectroscopic properties of doped and defective semiconducting oxides from hybrid density functional calculations. *Accounts Chem. Res.* **2014**, *47*, 3233–3241. [CrossRef] [PubMed]
13. Yu, W.L.; Zhang, J.F.; Peng, T.Y. New insight into the enhanced photocatalytic activity of N-, C- and S-doped ZnO photocatalysts. *Appl. Catal. B* **2016**, *181*, 220–227. [CrossRef]
14. Klingshirn, C.F. ZnO: Material, physics and applications. *Chem. Phys. Chem.* **2007**, *8*, 782–803. [CrossRef] [PubMed]
15. Qin, H.; Li, W.; Xia, Y.; He, T. Photocatalytic activity of heterostructures based on ZnO and N-doped ZnO. *ACS Appl. Mater. Interfaces* **2011**, *3*, 152–3156. [CrossRef]
16. Gautam, U.K.; Panchakarla, L.; Dierre, B.; Fang, X.; Bando, Y.; Sekiguchi, T.; Govindaraj, A.; Golberg, D.; Rao, C. Solvothermal synthesis, cathodoluminescence, and field- emission properties of pure and N- doped ZnO nanobullets. *Adv. Funct. Mater.* **2009**, *19*, 131–140. [CrossRef]
17. Bhirud, A.P.; Sathaye, S.D.; Waichal, R.P.; Nikam, L.K.; Kale, B.B. An eco-friendly, highly stable and efficient nanostructured p-type N-doped ZnO photocatalyst for environmentally benign solar hydrogen production. *Green Chem.* **2012**, *14*, 2790–2798. [CrossRef]
18. Perkins, C.L.; Lee, S.-H.; Li, X.; Asher, S.E.; Coutts, T.J. Identification of nitrogen chemical states in N-doped ZnO via X-ray photoelectron spectroscopy. *J. Appl. Phys.* **2005**, *97*, 034907. [CrossRef]

19. Molla, M.A.I.; Furukawa, M.; Tateishi, I.; Katsumata, H.; Kaneco, S. Fabrication of Ag-doped ZnO by mechanochemical combustion method and their application into photocatalytic Famotidine degradation. *J. Environ. Sci. Health Part A* **2019**, *54*, 914–923. [CrossRef]

20. Lu, J.; Zhang, Q.; Wang, J.; Saito, F.; Uchida, M. Synthesis of N-Doped ZnO by grinding and subsequent heating ZnO-urea mixture. *Powder Technol.* **2006**, *162*, 33–37. [CrossRef]

21. Mapa, M.; Gopinath, C.S. Combustion synthesis of triangular and multifunctional $ZnO_{1-x}N_x(x \leq 0.15)$ materials. *Chem. Mater.* **2008**, *21*, 351–359. [CrossRef]

22. Zong, X.; Sun, C.H.; Yu, H.; Chen, Z.G.; Xing, Z.; Ye, D.; Lu, G.Q.; Li, X.; Wang, L. Activation of photocatalytic water oxidation on N-doped ZnO bundle-like nanoparticles under visible light. *J. Phys. Chem. C* **2013**, *117*, 4937–4942. [CrossRef]

23. Prabakaran, E.; Pillay, K. Synthesis of N-doped ZnO nanoparticles with cabbage morphology as a catalyst for the efficient photocatalytic degradation of methylene blue under UV and visible light. *RSC Adv.* **2019**, *9*, 7509–7535. [CrossRef]

24. Ma, H.; Cheng, X.; Ma, C.; Dong, X.; Zhang, X.; Xue, M.; Zhang, X.; Fu, Y. Synthesis, characterization, and photocatalytic activity of N-doped ZnO/ZnS composites. *Inter. J. Photoenergy* **2013**, 625024. [CrossRef]

25. Molla, M.A.I.; Furukawa, M.; Tateishi, I.; Katsumata, H.; Kaneco, S. Studies of effects of calcination temperature on the crystallinity and optical properties of Ag–doped ZnO nanocomposites. *J. Compos. Sci.* **2019**, *3*, 18. [CrossRef]

26. Sakib, A.A.M.; Masum, S.M.; Hoinkis, J.; Islam, R.; Molla, M.A.I. Synthesis of CuO/ZnO nanocomposites and their application in photodegradation of toxic textile dye. *J. Compos. Sci.* **2019**, *3*, 91. [CrossRef]

27. Suna, S.; Chang, X.; Li, X.; Li, Z. Synthesis of N-doped ZnO nanoparticles with improved photocatalytical activity. *Ceram. Inter.* **2013**, *39*, 5197–5203. [CrossRef]

28. Khana, S.A.; Noreen, F.; Kanwal, S.; Iqbal, A.; Hussain, G. Green synthesis of ZnO and Cu-doped ZnO nanoparticles from leaf extracts of Abutilon indicum, Clerodendrum infortunatum, Clerodendrum inerme and investigation of their biological and photocatalytic activities. *Mater. Sci. Eng. C* **2018**, *82*, 46–59. [CrossRef]

29. Zheng, Y.; Chen, C.; Zhan, Y.; Lin, X.; Zheng, Q.; Wei, K.; Zhu, J.; Zhu, Y. Luminescence and photocatalytic activity of ZnO nanocrystals: Correlation between structure and property. *Inorg. Chem.* **2007**, *46*, 6675–6682. [CrossRef]

30. Wang, J.; Liu, P.; Fu, X.; Li, Z.; Han, W.; Wang, X. Relationship between oxygen defects and the photocatalytic property of ZnO nanocrystals in nafionmembranes. *Langmuir* **2008**, *25*, 1218–1223. [CrossRef]

31. Park, H.; Alhammadi, S.; Bouras, K.; Schmerber, G.; Ferblantier, G.; Dinia, A.; Slaoui, A.; Jeon, C.-W.; Park, C.; Kim, W.K. Nd-doped SnO_2 and ZnO for application in $Cu(InGa)Se_2$ solar cells. *Sci. Adv. Mater.* **2017**, *9*, 2114–2120. [CrossRef]

32. Molla, M.A.I.; Furukawa, M.; Tateishi, I.; Katsumata, H.; Suzuki, T.; Kaneco, S. Photocatalytic decolorization of dye with self–dye–sensitization under fluorescent light irradiation. *ChemEngineering* **2017**, *1*, 8. [CrossRef]

33. He, Y.; Wang, Y.; Zhang, L.; Teng, B.; Fan, M. High-efficiency conversion of CO_2 to fuel over $ZnO/g-C_3N_4$ photocatalyst. *Appl. Catal. B* **2015**, *168–169*, 1–8.

34. Molla, M.A.I.; Tateishi, I.; Furukawa, M.; Katsumata, H.; Suzuki, T.; Kaneco, S. Evaluation of reaction mechanism for photocatalytic degradation of dye with self-sensitized TiO_2 under visible light irradiation. *Open J. Inorg. Non-metallic Mater.* **2017**, *7*, 1–7. [CrossRef]